Analysis of turbulent wake behind a wind turbine

Kermani, Nasrin Arjomand; Andersen, Søren Juhl; Sørensen, Jens Nørkær; Shen, Wen Zhong

Published in:
Proceedings of the 2013 International Conference on aerodynamics of Offshore Wind Energy Systems and wakes (ICOWES2013)

Publication date:
2013

Document Version
Publisher's PDF, also known as Version of record

Analysis of turbulent wake behind a wind turbine

N. Arjomand Kermani[1], S. Andersen[1], J. Sørensen[1], W. Shen[1]

[1]Technical University of Denmark, Department of Wind Energy, Nils Koppels Alle, Building 403, 2800, Lyngby, **nsarjomand@gmail.com, jns@mek.dtu.dk, wzs@mek.dtu.dk**

Abstract

The aim of this study is to improve the classical analytical model for estimation of the rate of wake expansion and the decay of wake velocity deficit in the far wake region behind a wind turbine. The relations for a fully turbulent axisymmetric far wake were derived by applying the mass and momentum conservations, the self-similarity of mean velocity profile and the eddy viscosity closure.

The theoretical approach is validated using the numerical results obtained from large eddy simulations with an actuator line technique at 0.1% and 3% ambient turbulence level and ambient wind velocity of 10 m/s, and 0.1% ambient turbulence level and ambient wind velocity of 7 m/s. The obtained results showed that neglecting the nonlinear term of velocity in the momentum equation in the far wake region cannot be a fair assumption, unlike what is generally assumed in most of text books of fluid mechanics. Therefore the theoretical determination of the power law for the wake expansion and the decay of the wake velocity deficit may not be valid in the case of the wake generated behind a wind turbine with low ambient turbulence and high thrust coefficient. Although at higher ambient turbulence levels or lower ambient wind velocities (higher thrust coefficients), this trend may be improved due to the faster recovery of the wake and therefore closer values to the theoretical approach may be obtained. In addition, the assumption of self-similarity behavior of the mean velocity profile, when scaled with center line velocity deficit, could be correct in the far wake region of a wind turbine and low ambient turbulence levels.

1. Introduction

Modeling of wind turbine wakes has been a hot research topic during the past few years. Due to the generation of the wakes behind upstream wind turbines, the annual power production of a downstream wind turbine is decreased but at the same time the fatigue load of the turbine is increased significantly, compared to the performance of a free standing wind turbine. Therefore, developing an effective mathematical model for precisely simulating the wake behavior behind the wind turbine is highly desirable. Such model can be useful for the estimation of energy production, and life time of wind turbines and finally for optimization purposes.

Today, all the wake models that are used to predict the performance of wind turbines are either CFD based models or kinematic wake models. The CFD based models are highly advanced which are able to predict the flow behaviors with a high degree of accuracy, but they are very time consuming and require massive computer resources. On the other hand, most of the kinematic wake models are mainly based on mass and momentum conservations. These models are basically calibrated with several empirical coefficients obtained from specific field measurements and therefore have limitations. Although the kinematic wake models use explicit representations of turbulence and its impact on the wake expansion, they have not been able to produce convincingly better predictions.

For many years it was imagined that the turbulence tends to forget its origin and in this context, the self-preserving state in the flow is obtained, when it becomes asymptotically independent of its initial conditions. Consequently, different types of flows, like wakes and other free turbulent shear flows can grow asymptotically at the same rate which is independent of their generators. This classical self-preservation approach was questioned for the first time in 1989 by George [1], who proposed a new methodology called "equilibrium similarity" analysis. In this new method, George [1] argued that the axisymmetric wake will reach a self-similarity state with respect to the mean velocity profile, if scaled with the centerline wake velocity deficit. Therefore, independent of how far downstream the wake moves or how large the Reynolds number is [1],the properly normalized mean velocity profiles with the centerline wake velocity deficit always collapse onto a unique curve, while the spreading rate and higher turbulence moments will appear differently, depending on their source. In 2003, Johansson et al. [2] validated the mentioned theory by using the experimental data for axisymmetric wake obtained by Johansson et al. [3, 4], the experimental data for axisymmetric wake behind five different generators obtained by Canon [5], and the direct numerical simulation obtained by Gourlay et al. [6].
In addition, by using kinetic energy equation and ad hoc assumptions about the dissipation, George [1] showed that the Reynolds number is the main factor in determining the rate of the axisymmetric wake width (either $\sim x^{\frac{1}{3}}$ or $\sim x^{\frac{1}{2}}$) which were always a doubt. By removing the ad hoc assumptions and using the Reynolds averaged equations, instead of kinetic energy Johansson et al. [2] revised this theory. Based on these studies, two different equilibrium similarity solutions were obtained for the two different cases of very high and low local Reynolds numbers in the axisymmetric wake.

Kinematic wake models are analytical models which gain a considerable attention for predicting the flow behavior behind the wind turbines due to their simplicity and low computational cost [7]. As reviewed in Vermeer et al. [8] and Crespo et al. [7] this approach was introduced for the first time by Lissama [9] and up to now a lot of researchers work on developing these models. N.O Jensen model [10, 11] is a single wake model based on the balance of momentum which describes the wake behind a wind turbine in terms of Guassian distribution of wake velocity deficit and the linear expansion of the wake. Larsen model [12, 13] is another kinematic model based on mass and momentum conservation together with the assumption of Prandtl's turbulent boundary layer equations and similarity. This model is described for two different levels of approaches where in the first order model, two power lows of 1/3 and -2/3 are obtained for the wake expansion and wake velocity deficit respectively while in the second order level these values changed to more complicated relations. In 2006, Frandsen [14] suggested a new analytical model based on the mass and momentum conservations, and the similarity assumption for prediction of the flow behavior in the wake for any size of wind farms. Compared to the previous models, this model is able to handle more condition close to the reality, but it is still required to be evaluated and calibrated based on the measurements. Most of the kinematic models that are used for predicting the wake behind wind turbine are based on self-similarity assumption of the mean velocity profile. However no one has shown the accuracy of this behavior in the far wake region of wind turbine and the possibility of having a unique profile independent of its source. In addition, these models are mainly based on the mass and momentum conservations, but none of them has considered the turbulent kinetic energy or the Reynolds stress equations, that may lead to more accuracy in prediction of the flow behaviors. Also there are still a lot of contradictory arguments regarding the spreading rate of the wake, and a lot of uncertainty about applying the initial conditions of the wake in these models.

The aim of the present study is to improve the classical analytical model for estimating the rate of wake expansion and the decay of wake velocity deficit in the far wake region behind a wind turbine. The asymptotic behavior of the far wake is investigated as well as a detailed theoretical approach is presented in the paper. The model has been developed by applying the mass and momentum conservations and Reynolds shear stress. Finally, a closed form solution is derived for centerline and radial wake velocity deficit, wake width, mean velocity profile, and relations for coefficients by adopting the self-similarity of mean velocity profile and utilizing the eddy viscosity closure scheme in the description of turbulent stresses.

The theoretical work is verified and validated against the results obtained from Navier-Stokes/Actuator Line simulations with large eddy simulation at 0.1% ambient turbulence and an ambient wind velocity of $U_\infty = 10\ m/s$. In addition, the effects of ambient turbulence level and thrust coefficient on the wake recovery and the flow behaviors are investigated by analyzing the flow parameters obtained from the numerical data at two different ambient turbulence levels of 3%, 6% and an ambient wind velocity of $U_\infty = 10\ m/s$ s, and 0.1% ambient turbulence level and an ambient wind velocity of $U_\infty = 7\ m/s$.

2. Methods

2.1 Theoretical approach

To make theoretical approach, the wake behind a wind turbine is assumed to be incompressible, steady and fully turbulent. However these assumptions may not be correct when looking at the instantaneous behavior of the wake flow; they will be acceptable if a relatively long time series of the data is considered. In addition the inflow is assumed to be uniform and stationary with time, and the ground effects and pressure gradient outside the wake are negligible.

2.1.1 Basic model equations

The wake is described in cylindrical coordinates (x, r) with the axial and radial velocity components (u, v) respectively. According to the above assumptions, the continuity equations for the mean and fluctuating velocity together with the stream-wise momentum equation can be rewritten as follows

$$\frac{\partial(\bar{u})}{\partial x} + \frac{1}{r}\frac{\partial(r\bar{v})}{\partial r} = 0 \quad ; \quad \frac{\partial(u')}{\partial x} + \frac{1}{r}\frac{\partial(rv')}{\partial r} = 0 \tag{1.}$$

$$\left(\bar{u}\frac{\partial\bar{u}}{\partial x} + \bar{v}\frac{\partial\bar{u}}{\partial r}\right) = -\frac{1}{r}\frac{\partial(r\overline{u'v'})}{\partial r} - \frac{\partial\left(\overline{u'^2}\right)}{\partial x} + \nu_s\left(\frac{\partial}{\partial x}\frac{\partial\bar{u}}{\partial x} + \frac{1}{r}\frac{\partial}{\partial r}\left(r\frac{\partial\bar{u}}{\partial r}\right)\right) - \frac{1}{\rho}\frac{\partial\bar{p}}{\partial x} \tag{2.}$$

where $u'$and v' are the fluctuating parts of u and v, and a bar over the quantities denotes time average. The third and fourth terms on the right hand side of Eq. 2 correspond to the viscous terms and the last term on the right hand side of the Eq. 2 is the pressure term. The equations of motion are simplified in the far wake region by analyzing the orders of magnitude and discarding many terms that are relatively small. In order to do so, two velocity scales (U_∞ and $\overline{u_s}$) and two length scales L and δ are used in the far wake, which stand for the ambient wind velocity, the cross sectional wake velocity deficit in the axial direction, and the stream-wise and cross-stream length scales, respectively. $\overline{u_s}$ is the cross sectional wake velocity deficit defined as the difference between U_∞ and the wake velocity in the axial direction $\overline{u}$, while $\overline{U_s}$ is the centerline wake velocity deficit. In addition, δ is equal to the perpendicular distance from the wake centerline to the wake edge (half of the wake width) and can be defined as two times of the distance from the centerline to where $U_\infty - \bar{u}$ is about $\frac{1}{2}\overline{U_s}$. For more information about the order of magnitude analysis the reader is referred to [15]. Consequently, for fully turbulent axisymmetric far wake Eq. 2 could be simplified as

$$(U_\infty)\frac{\partial}{\partial x}(\overline{u_s}) = -\frac{1}{r}\frac{\partial(r\overline{u'v'})}{\partial r} + \nu_s\frac{1}{r}\frac{\partial}{\partial r}(r\frac{\partial}{\partial r}\overline{u_s}) \tag{3.}$$

2.1.2 Momentum thickness and self-similarity analysis

An infinitely large cylindrical control volume surrounding the rotor is chosen with x-axis as the symmetry axis of the control volume. Therefore, using the previously defined assumptions, neglecting the shear forces acting on the control volume, and applying continuity equation the momentum theory applied to the chosen control volume can be simplified with respect to the mean velocity (neglecting the fluctuating terms) as follows,

$$2\pi\rho\int_0^\infty \bar{u}(U_\infty-\bar{u})rdr=\bar{T}\quad where\quad \bar{T}=\frac{1}{2}\rho C_T U_\infty^2 A=\frac{1}{2}\rho C_T U_\infty^2\frac{\pi}{4}D^2 \tag{4.}$$

where ρ, $\overline{T}$, C_T, A and D are the air density, thrust, thrust coefficient, rotor area and rotor diameter respectively. Therefore, based on the definition of momentum thickness (showed below) and Eq. 4, the relation between momentum thickness and thrust can be found as

$$\theta^2=\int_0^\infty\frac{\bar{u}}{U_\infty}\left(1-\frac{\bar{u}}{U_\infty}\right)rdr=\frac{\bar{T}}{2\pi\rho U_\infty^2}\ \rightarrow\ \theta^2=\frac{1}{4\pi}C_T A=\frac{1}{16}D^2C_T \tag{5.}$$

Considering the self-similarity assumption, the following relation can be written for the mean velocity profile and the Reynolds stress, where $u'v'$, $f(\eta)$, R_s, g and η are the Reynolds stress, the mean velocity deficit, the Reynolds shear-stress scaling function and profile, and the dimensionless similarity coordinates, respectively.

$$U_\infty-\bar{u}=\overline{U_s(x)}f(\eta)\ ;\ \ \overline{u_s(x)}=\overline{U_s(x)}f(\eta)\ ;\ \ -\overline{u'v'}=R_s(x)g(\eta)\ \ where\quad \eta=\frac{r}{\delta}\ \ and\ \ \delta=\delta(x) \tag{6.}$$

By substituting Eqs. 6 in Eq. 4 and neglecting the nonlinear term of the momentum equation (due to the far wake modelling) Eq. 4 can be simplified as follows, see also Johansson et al. [2]

$$2\pi\rho\int_0^\infty\left(U_\infty\overline{u_s(x)}-\overline{u_s(x)^2}\right)rdr=\bar{T}=2\pi\rho U_\infty^2\theta^2\quad\rightarrow\quad\overline{U_s}\delta^2\int_0^\infty\eta f(\eta)d\eta=\bar{T}=U_\infty\theta^2=Const \tag{7.}$$

By using Eq. 4 and Eqs. 6 in Eq. 3 and repeating similar analysis for Reynolds stress equations together with the elimination of viscous terms, Johansson et al. found the two power laws of 1/3 and -2/3 for the wake expansion and the decay of wake velocity deficit for high Reynolds solution in the far wake region, respectively as

$$\frac{\delta_*}{\theta}=a\left(\frac{x}{\theta}\right)^{\frac{1}{3}}\ ;\ \ \frac{\overline{U_s}}{U_\infty}=b\left(\frac{x}{\theta}\right)^{-\frac{2}{3}};\ and\quad x=x-x_0\ \ where\quad\delta_*^2=\lim_{R\to\infty}\frac{1}{U_s}\int_0^R(U_\infty-\bar{u})rdr \tag{8.}$$

where the coefficients (a and b) and the virtual origin of the far wake (x_0) are highly dependent on initial conditions. However, Eqs. 7 can be written based on δ (half of the wake width), where the coefficient (a) will have a different value compared to the case of δ_*(displacement thickness).

2.1.3 Mean and radial velocity profile

By using the relations in Eqs. 8 into Eq. 3, introducing the eddy viscosity in the form of $-\overline{u'v'}=\nu_T\frac{\partial\bar{u}}{\partial r}$, and employing the relations in Eqs. 7, the following equations were found for the mean velocity profile (f), and the relation between *a* and *b* coefficients, respectively.

$$f=\exp\left(-\frac{1}{6}\alpha\eta^2\right)\ \ where\ \alpha=\frac{aR_T}{b}\ \ ;\ \ and\ \ b=1/a^2 \tag{9.}$$

where $R_T = \frac{\overline{U_s}\delta}{\nu_T}$, is the turbulent Reynolds number which is assumed to be constant. By using Eqs. 6 and 8 in Eq. 1, the following relations will be obtained for the radial velocity profile. For more detailed information regarding the above calculation, the reader is referred to [15].

$$\overline{u_r} = \frac{\delta}{\eta}\, U_\infty \theta^{\frac{2}{3}} x^{-\frac{5}{3}} \left[\frac{b}{3}\eta^2 f(\eta)\right] \qquad (10.)$$

2.2 Numerical approach

The numerical model used here is a multi-block finite volume code combined with the Actuator Line technique. The Actuator Line model was developed by Sørensen and Shen [16] and later on implemented into the three dimensional Navier-Stokes solver EllipSys3D, developed by Michelsen [17, 18] and Sørensen [19]. In this code, the discretized incompressible Navier-Stokes equations, in general curvilinear coordinates, are solved by using the block structured finite volume approach [20]. In the actuator line model each blade is represented by a line and the loading is distributed radially along the lines representing the blade forces. The kinematics of the wake is determined by a fully three dimensional Navier-Stokes equations, whereas the loading on each blade, is determined by using tabulated airfoil data.

In addition, for Large Eddy simulation (LES), sub grid scale (SGS) models is used to model eddies of size smaller than the grid size. Therefore, the equations are obtained by filtering the time dependent Navier-Stokes equations in the physical space. The eddy-viscosity-based mixed scale model in [20] is used to model the small scales. In addition the Mann turbulence model [21] is used to produce the desired ambient turbulence for the simulations.

2.2.1 Computational domain and boundary conditions

The computations were carried out in a Cartesian computational mesh of about 14 million grid points (216×40^3) with dimensions 48R in the axial direction (x), 20R in the vertical direction (y) and 20R in the lateral direction (z). The actuator lines were rotating in the $y - z$ plane and located at 8R downstream of the inlet and the origin of rotation is the center of the plane. Therefore, the computational domain has covered the region extending from 8R before the rotor plane to 40R downstream of the rotor in the flow direction, and 10R from the rotor center in the y and z directions.

The grid points of the computational mesh are highly concentrated around and downstream of the rotor and distributed equally in order to resolve the strong gradients in the vicinity of the rotor and to maintain the generated flow structure in the wake simultaneously. While out of this region, they stretched away towards the outer boundaries. Note that in this simulation 16 grid cell is used to resolve a rotor radius in the equidistant region. The grid configuration is divided into 216 blocks (3×3 in cross-flow and 24 in flow direction) with 40^3 grid points in each block. Figure 1 shows the block configuration which is used in the simulations.

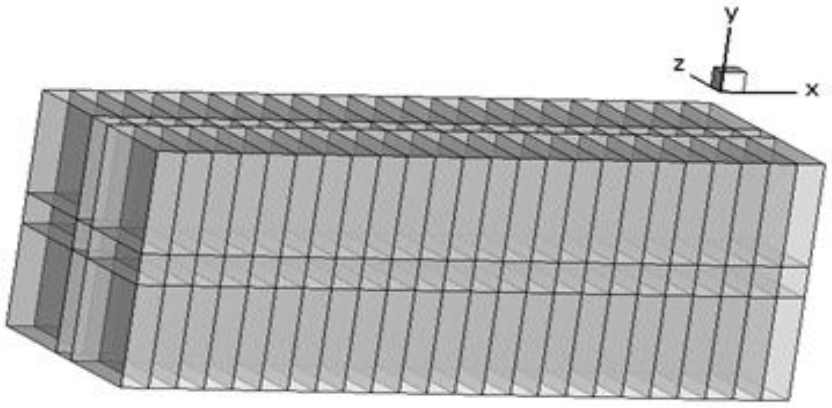

Figure 1: Grid configuration used in numerical simulation.

The boundary conditions used here are

Dirichlet boundary conditions with, constant and uniform flow velocity component (V_x) and zero velocity component in the y and z directions (V_y and V_Z) at the inlet ($x/R = 0$), a convective boundary condition at the outlet ($x/R = 48$), and periodic boundary condition at the lateral ($z/R = -10,\ z/R = 10$).

2.2.2 Wind turbine characteristics and flow parameters

The flow field past a 2.75 MW variable speed pitch regulated "NM80" stiff wind turbine equipped with three LM38.8 blades which are constructed with NACA634XX airfoils, is simulated. The rotor diameter of the wind turbine is equal to 80 m and it runs with the rated speed of 17.2 rpm. In addition, two different uniform inflow velocities of $U_\infty = 7 \text{ and } 10\ m/s$ with air density of $\rho = 1.22 \frac{kg}{m^3}$ are used in the presented work. Since the turbine's data is confidential, the detailed data are not allowed to be presented.

3. Results and discussions

The computation for 0.1% ambient turbulence and ambient wind velocity of 10 m/s (corresponding to $C_T = 0.75$ and a tip speed ratio of $\lambda = 7.78$) has been run first to examine the accuracy of the assumptions and then verify and validate the main characteristics of the flow predicted by the theoretical approach. Later on in the study, the simulations were repeated for 3 different conditions of (3%, and 6% ambient turbulence level and $U_\infty = 10\ m/s$) together with (0.1% ambient turbulence level and $U_\infty = 7\ m/s$ corresponding to $C_T = 0.86$ and a tip speed ratio of $\lambda = 11.42$) in order to evaluate the effects of ambient turbulence and wind turbine rotor aerodynamics on the flow behaviors.

The computations have run on a cluster where three component of dimensionless wake velocity deficit in axial, cross-sectional directions ($u/U_\infty, v/U_\infty, w/U_\infty$) are saved in $y-z$ planes, at the distances of $\frac{x}{D} = 1, 2, 3, 4, 5, 6, 7, 8, 9, 10, 11, 12, 13, 14, 15, 16, 17, 18, 19$ behind the wind turbine. All the data have been read and analyzed in Matlab software with time step duration of 0.5 seconds.

Figure 2 shows the dimensionless axial wake velocity deficit obtained from numerical simulation for 0.1% ambient turbulence level and $U_\infty = 10\ m/s$ averaged in time between 3.3 to 39 minutes in $y-z$ plane at four

different distances of $\frac{x}{D} = 3, 6, 11, 18$ behind the wind turbine. It can be seen from Figure 2, the decreasing and increasing trend of the centerline wake velocity deficit and the wake width as the wake evolves downstream. In addition, it is clear from the figure that the wake velocity deficit reaches the axisymmetric condition

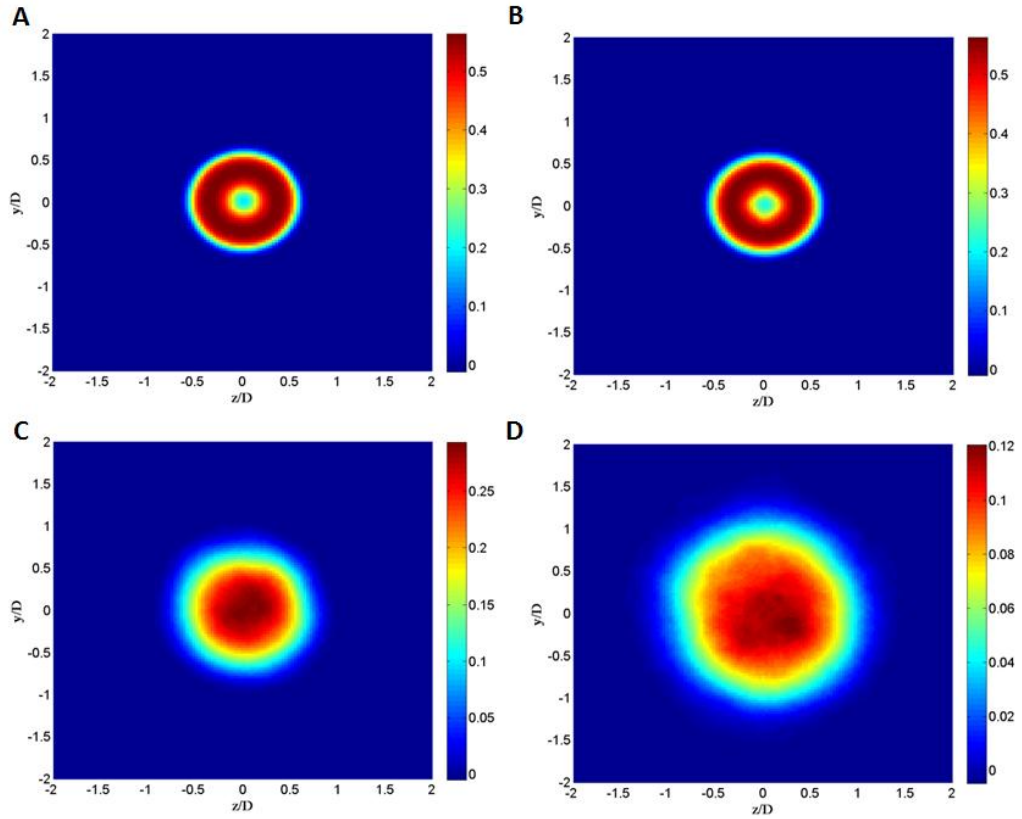

Figure 2: Dimensionless wake velocity deficit for 0.1% ambient turbulence and an ambient wind velocity of 10 m/s, at (A) x/D=3, (B) x/D=6, (C) x/D=11, (D) x/D=18 (obtained from numerical simulations)

3.1 Verification of steady state condition

Figure 3 shows the variation of the time-averaged dimensionless centerline wake velocity deficit ($\frac{\overline{U_s}}{U_\infty}$) by increasing the time interval of 0.25 min at each step, for 0.1% ambient turbulence level and $U_\infty = 10\ m/s$. The first point in Figure 3, corresponds to the value of centerline wake velocity deficit averaged by time between ($T_{avr} = 3.3\ to\ 30$ min). These relatively small variations of the time-averaged dimensionless wake velocity (less than 5%) shows the fact that the simulation time was large enough for the wake to reach the steady state conditions, and therefore satisfying the assumptions used in the theory.

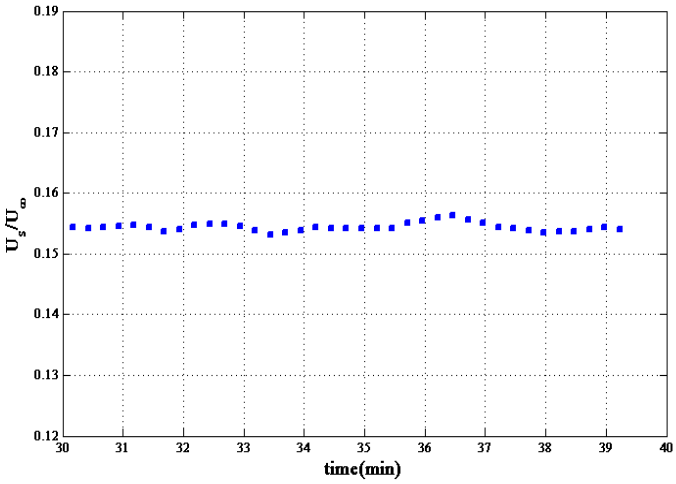

Figure 3: Variation of dimensionless centerline wake velocity deficit averaged in different time intervals, for 0.1% ambient turbulence and an ambient wind velocity of 10 m/s (obtained from numerical simulations)

3.2 Investigation of cross-sectional parameters

Figure 4 shows the cross-sectional profile of the dimensionless wake velocity deficit and the turbulence intensity at different distances behind the wind turbine for 0.1% ambient turbulence level and $U_\infty = 10\ m/s$. Note that the values shown for the dimensionless wake velocity deficit profile and turbulence intensity in Figure 4 correspond to the tangential averaged values between $\Delta\theta = 0$ to π ; and $-\pi$ to 0 of these quantities.

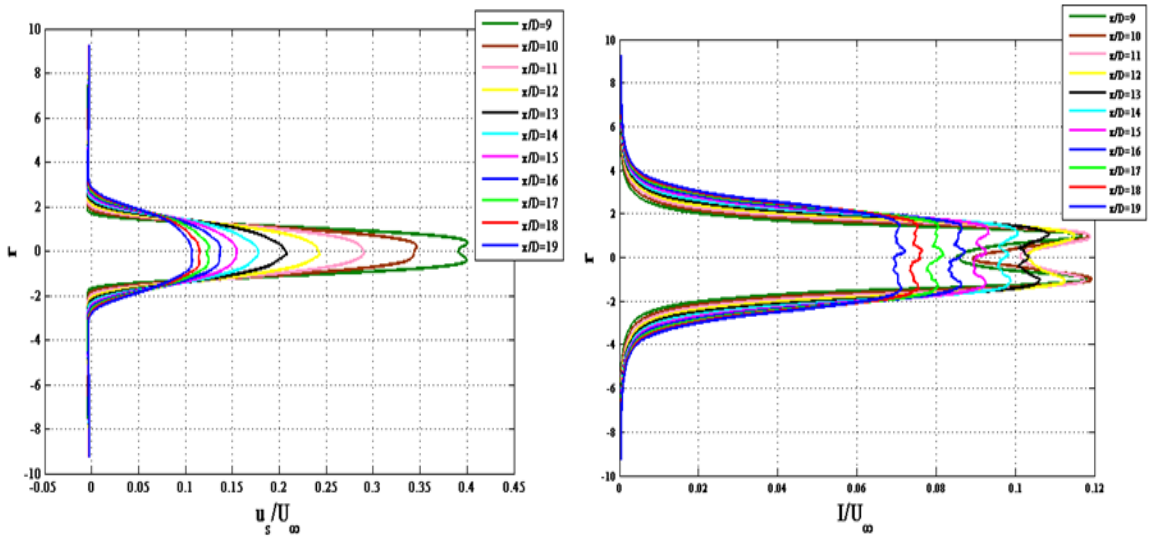

Figure 4: Cross-sectional dimensionless wake velocity deficit (left) turbulence intensity (right) at different distances behind the wind turbine for 0.1% ambient turbulence and an ambient wind velocity of 10 m/s (obtained from numerical simulations)

Figure 4 shows that both dimensionless cross-sectional profiles of wake velocity deficit and turbulence intensity are decreased as the wake evolves downstream. Figure 4 also shows that the dimensionless velocity deficit

profiles reach "a point of balance" and become approximately "bell-shaped with having a maximum approximately in the center of the wake". Since, in the transitional and far wake region the new turbulent fluctuations are generated by the radial shear flow, there is less generation of turbulence in the center of the wake. However, in this condition the turbulent diffusion is the dominant mechanism which transports the turbulent fluctuations to the center of the wake and therefore leads to fair approximation of the turbulence fluctuations with bell-shaped form.

3.3 Variation of flow parameters for different initial conditions

Comparing the figures of time-averaged wake velocity deficit profile shows that the transitional region (the region where the annular shear layer of the near wake is finished) for different ambient turbulence levels of 0.1%, 3% and 6% and $U_\infty = 10\ m/s$ is started at approximately $\frac{x}{D} \geq 9$, $\frac{x}{D} \geq 5, \frac{x}{D} \geq 3$ respectively, while for 0.1% ambient turbulence level and $U_\infty = 7\ m/s$ the transitional region will start at $\frac{x}{D} \geq 6$. Figure 5 shows the logarithmic behavior of dimensionless half of wake width and centerline wake velocity deficit in transitional and far wake region of wind turbine for 0.1%, 3%, 6% ambient turbulence levels and $U_\infty = 10\ m/s$, and 0.1% ambient turbulence level and $U_\infty = 7\ m/s$ corresponding to the time averaging of 35.7 min, 11.7 min, 11.7 min, and 35.2 min, respectively.

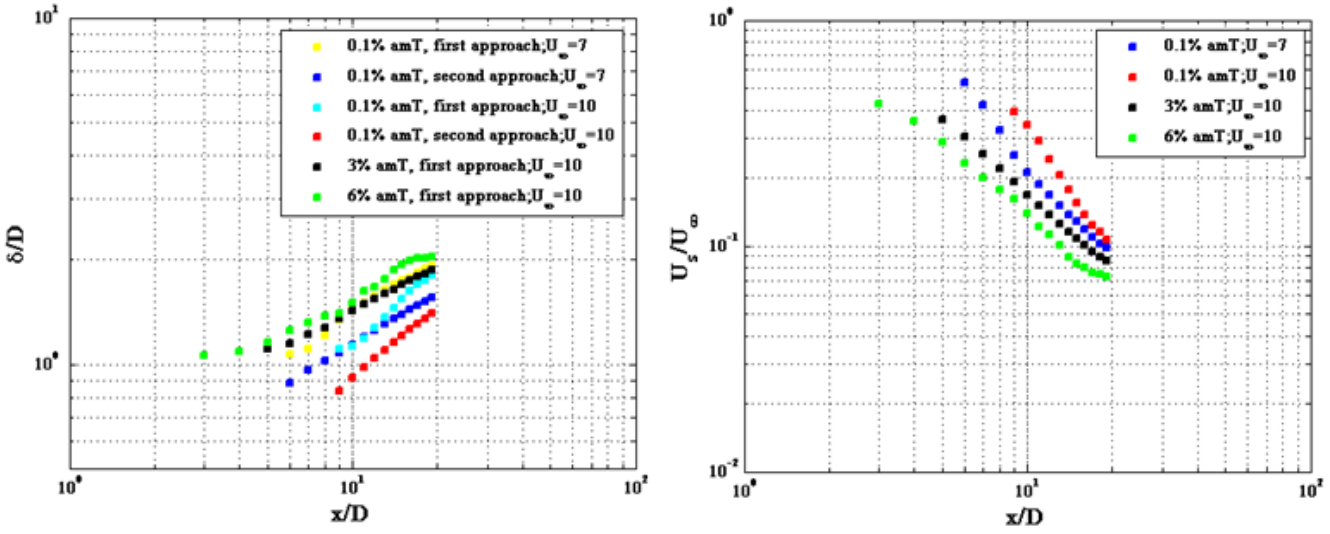

Figure 5: Log-log plot of dimensionless half of wake width (left) and the centerline wake velocity deficit (right) in transitional and far wake region, for different initial conditions

The wake width is calculated in two ways:

First approach (FA): Calculate δ to be two times of the distance from the wake centerline to which $\bar{u} - U_\infty$ is about $\frac{1}{2}\overline{U_s}$, where $\overline{U_s}$ is the time-averaged dimensionless wake velocity deficit at the center of y-z plane.

Second approach (SA): Calculate δ where $\frac{\bar{u}}{U_\infty} < 1$ and $\bar{u}$ stands for dimensionless wake velocity.

Comparing the values of dimensionless half of wake width for example at 0.1% and $U_\infty = 10\ m/s$ with Figure 2 seems that the estimations of $\frac{\delta}{D}$ based on the (first approach) is overestimated. Therefore, $\frac{\delta}{D}$ for 0.1% ambient

turbulence level is also calculated based on the second approach. Comparing the new values of $\frac{\delta}{D}$ with Figure 2 shows that the second approach might lead to more accurate results (for more details regarding calculation of $\frac{\delta}{D}$ the reader is referred to [15], however due to uncertainties at the edges of the wake , $\frac{\delta}{D}$ for ambient turbulence level larger than 0.1% is only calculated based on the second approach. In addition, the points related to x/D>17 may be effected by boundary conditions and therefore the last two points are not considered in further calculations in the study.

Comparing the amount of dimensionless half of wake width and centerline wake velocity deficit in Figure 5 shows that by increasing the ambient turbulence level, the decay of the centerline wake velocity deficit and the rate of wake width expansion will increase. Therefore, it can be concluded that increasing ambient turbulence level will lead to faster recovery of the wake. This could easily be explained by transferring of more momentum into the wake due to the larger gradient between the inside and outside of the flow, in the case of larger ambient turbulence levels. In addition, it can be seen from Figure 5 that for 0.1% ambient turbulence level by decreasing the ambient wind velocity (higher thrust coefficients), the wake recovery will be faster, but still slower than 3% ambient turbulence level.

In order to find the location where the far wake starts, the dimensionless centerline turbulence intensity ($\frac{I_s}{U_\infty}$) is plotted at different distances behind the wind turbine under different initial conditions, where I_s is defined as $\frac{I_s}{U_\infty} = \sqrt{\overline{u'^2}/U_\infty^2}$, and u' is the fluctuating wake velocity deficit.

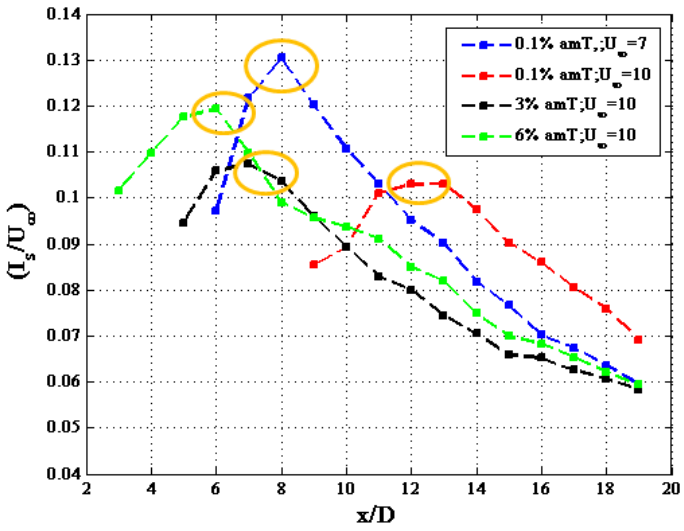

Figure 6: Centerline turbulence intensity at different distances behind the NM80 wind turbine under different initial conditions

It can be observed from Figure 6 that $\frac{I_s}{U_\infty}$ has increasing trend up to a certain level but after that it starts to decrease by increasing the distances. The main reason of that could be explained by the idea that in the near wake region, the turbulence level of the wake is mainly contributed from the ambient turbulence level in front of the turbine and the turbulence generated by the wind turbine rotors. From this region until the end of transitional region, the turbulence which is generated by the radial flow shear will start to affect the flow. Therefore,

dissipation starts to drain turbulent energy and the wake width increases while the velocity deficit is being reduced. This process may explain the gradual reduction of the increasing trend in both terms of $\frac{\overline{u'^2}}{U_\infty^2}$ as the wake evolves from the transitional region to the far wake, where the diffusion will be the dominant term and the turbulence will start to decrease considerably. Therefore, it is possible to find from Figure 6 that the end of the transitional region and therefore, beginning of the far wake will be at approximately $\frac{x}{D} \geq 13, \frac{x}{D} \geq 9, \frac{x}{D} \geq 8, \frac{x}{D} \geq 7$ for T=0.1% and $U_\infty = 10\ m/s$, T=0.1% and $U_\infty = 7 m/s$, T=3%and 6% ambient turbulence levels and $U_\infty = 10\ m/s$, respectively.

3.4 Power laws for centerline wake velocity deficit and half wake width

The accuracy of the two power laws of $\frac{1}{3}$ and $-\frac{2}{3}$ obtained in theoretical approach for the rate of wake expansion and decay of wake velocity deficit, are validated by numerical results. In order to do that these two powers ($\frac{1}{3}$ and $-\frac{2}{3}$) are also considered as two unknowns (α and β) in Eq. 8 as following,

$$\frac{\delta}{D} = A\left(\frac{x - x_0}{D}\right)^{\alpha} \quad ; \quad \frac{\overline{U_s}}{D} = B\left(\frac{x - x_0}{D}\right)^{\beta} \tag{11.}$$

It should be taken into consideration that the momentum thickness has decreasing trend in our data, due to the effect of pressure gradient, instead of a constant value which is required in Eqs. 8 (For more information, the reader is referred to [15]). Therefore, in order to obtain higher accuracy, Eqs. 8 are only non-dimensionalized based on the turbine diameter (D) in Eqs. 11 which means that he two coefficients *a* and *b* are now changed to A and B respectively. However, the relation between a, b in Eqs. 8 and A, B in Eqs, 11 could be easily found by using Eq. 5 as following.

$$A = 0.4\, C_T^{\frac{1}{3}} a \quad and \quad B = 0.4 C_T^{\frac{1}{3}} b \tag{12.}$$

In addition, it is also important to mention that in Eqs. 11, δ_* is substituted by δ which seems to give more accurate results. This means that the relation between a and b coefficients in Eqs. 9 ($b = 1/a^2$) is now changed to ($b = constant * 1/a^2$), since δ_* is the choice of δ, so that the integral in Eqs.7 ($\int_0^\infty \eta f(\eta) d\eta$) will be equal to unity.

However in Eq. 11 the system is not closed and the number of unknowns are different from the number of equations. Thus, in order to determine the unknowns, the problem is optimized and the best curve fitted with the numerical data based on the least square technique is found. The optimization process was down in Matlab by using "lsqcurvefit (f0, x00, xdata, Us)" and "lsqcurvefit (f0, x00, xdata, δ)" simultaneously, where f0 is defined as f0 = @(x,xdata)x(1)*(xdata-x0).^x(2), 'x','xd'; xdata corresponds the non-dimensionalized distances $\frac{x}{D}$ behind the rotor, and x0 and x00 are the virtual origin of the wake and initial value respectively. The previously mentioned "lsqcurvefit "will start at x00 and find the coefficient x to best fit the non-linear function f0 (x, xdata) to the data Us and δ ($ydata$) based on the least-square technique [22] as shown in Eq. 13.

$$\min_x \| F(x_i, xdata) - ydata \|_2^2 = \min_x \sum_i (F(x_i, xdata) - ydata_i)^2 \tag{13.}$$

Since X_0 is the joint term in both relations shown in Eq. 11, therefore it sets as an independent parameter in the non-linear function (f0), and consequently the problem is optimized based on this parameter for both quantities

of dimensionless centerline wake velocity deficit and half wake width at the same time. Moreover, optimization processes show that the problem is quite sensitive between the two distances where the transitional region is finished and the far wake is started. However it is not really possible to find the exact distance where the far wake starts. Therefore in order to have reliable results, which could be able to give close trend at both distances, the final solutions are chosen based on optimization of the average squared 2-norm of residuals of dimensionless centerline wake velocity deficit and half wake width between these two distances. Figure 7 shows the fitted curve with numerical data of dimensionless half wake width and centerline wake velocity deficit for different values of $\frac{x_0}{D} = 3$ to 8, 0.1% ambient turbulence level and $U_\infty = 10\ m/s$.

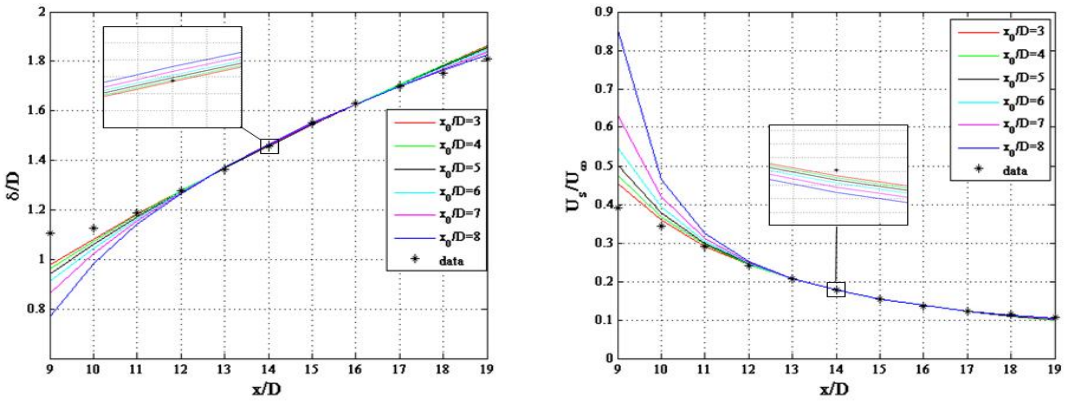

Figure 7: Fitted curve with numerical data of dimensionless half of wake width (left) and dimensionless centerline wake velocity deficit (right), for different x0/D values, 0.1% ambient turbulence level, and $U_\infty = 10\ m/s$

The results obtained from the optimization process for 0.1% and 3% ambient turbulence level and $U_\infty = 10\ m/s$ are as following. It should be taken into consideration that $\frac{\delta}{D}$ is calculated based on the second and first approach for ambient turbulence level of 0.1% and 3% respectively, in order to get the most reliable results.

***o*. 1%**: $\|residual\|_2^2 = 7.04E-06$; $\beta = -1.28$; $\alpha = 0.44$; $B = 3.06$; $A = 0.43$; $\frac{x_0}{D} = 4.84 \rightarrow \frac{\delta}{D} \sim \left(\frac{x}{D}\right)^{\frac{1}{2.27}}$; $\frac{U_s}{U_\infty} \sim \left(\frac{x}{D}\right)^{-\frac{2}{1.57}}$

3%: $\|residual\|_2^2 = 1.0674E-04$; $\beta = -1.01$; $\alpha = 0.39$; $B = 1.51$; $A = 0.6$; $\frac{x_0}{D} = 1.15 \rightarrow \frac{\delta}{D} \sim \left(\frac{x}{D}\right)^{\frac{1}{2.6}}$; $\frac{U_s}{U_\infty} \sim \left(\frac{x}{D}\right)^{-\frac{2}{1.98}}$

The above results show that the power which is obtained for the decay of centerline wake velocity deficit is far from the theoretical approach, while, the rate of wake expiation is a value between the two values which have been determined by Johansson et al. [2], for the two similarity equilibriums. However, for higher ambient turbulence the power laws become closer to the theoretical approach.

In addition, repeating the optimization processes for 0.1% ambient turbulence level and $U_\infty = 7\ m/s$ gave the following results

$\|residual\|_2^2 = 2.89E-04$; $\beta = -1.07$; $\alpha = 0.36$; $B = 1.78$; $A = 0.56$; $\frac{x_0}{D} = 2.97 \rightarrow \frac{\delta}{D} \sim \left(\frac{x}{D}\right)^{\frac{1}{2.8}}$; $\frac{U_s}{U_\infty} \sim \left(\frac{x}{D}\right)^{-\frac{2}{1.86}}$

Comparing the above results with the other two cases shows that the values obtained for the powers will become closer to the ones predicted by the theoretical approach as the wake recovers faster. However, comparing the rated of wake expansion for 0.1% ambient turbulence level and $U_\infty = 7\ m/s$ with 3% ambient turbulence level and $U_\infty = 10\ m/s$ shows a bit contradictory result. The main reason could be the fact of applying the first approach for estimation of the wake expansion at 3% ambient turbulence level and a relatively short time series of this simulation.

The difference between the results obtained from the optimization processes compared to theoretical approach might be due to the fact of neglecting of the nonlinear term of velocity deficit (the second term in the left side of Eq. 7). Figure 8 shows the percentage of the nonlinear term in the momentum integral in the transitional and far wake region behind the wind turbine for 0.1% and 3% ambient turbulence levels and $U_\infty = 10\ m/s$ and 0.1% ambient turbulence level and $U_\infty = 7 m/s$. As it is seen for 0.1% ambient turbulence, the percentage in the far wake region (x/D <12) is larger than 10, meaning that the theoretical approach might not be correct at this ambient turbulence level and wind speed. However, this trend improves by decreasing the ambient wind velocity or increasing the ambient turbulence level, due to the faster recovery of the wake.

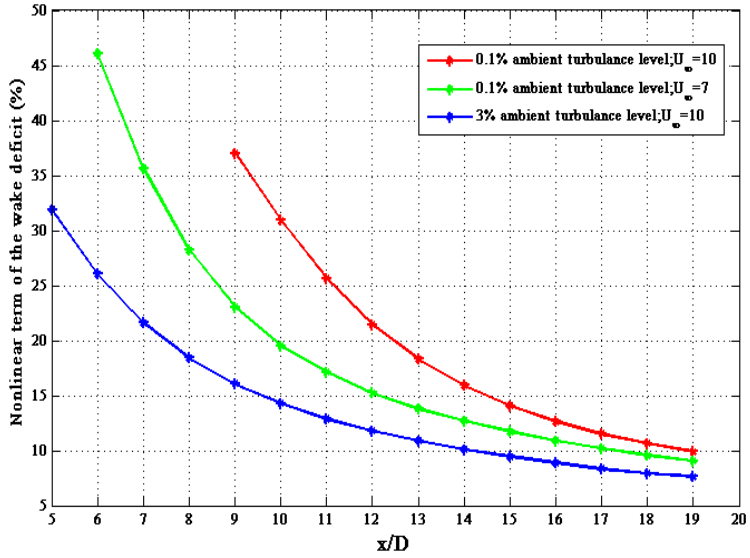

Figure 8: Estimation of the nonlinear term of the wake deficit in the momentum integral

To that end, it is also interesting to find the relations between β and α, as a function of thrust coefficient for 0.1% ambient turbulence level, Figure 9 shows these relations.

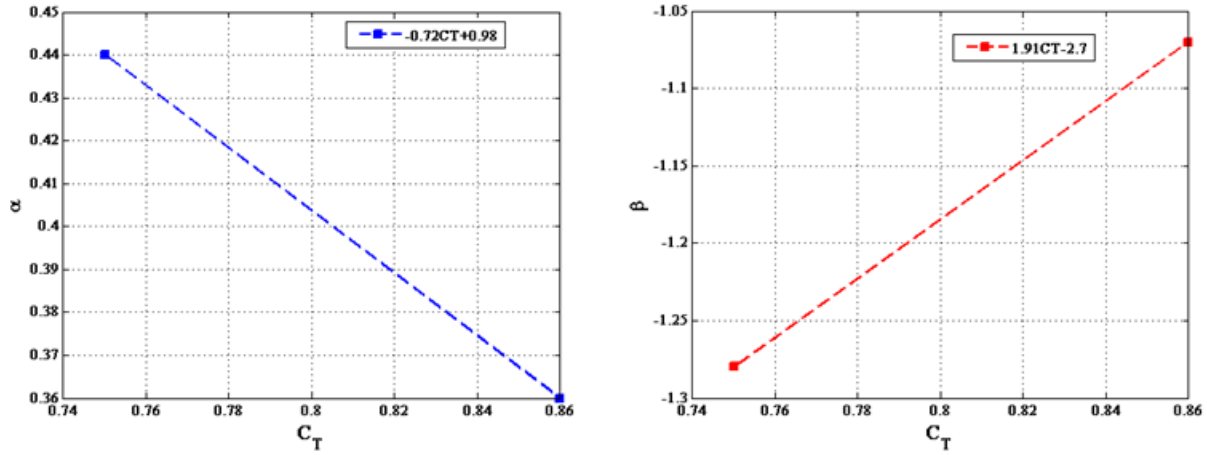

Figure 9, The relation between changes of β and α by the thrust coefficient, for 0.1% ambient turbulence level

3.5 Verification of the self-similarity behavior in the far wake

In order to verify the self-similarity behavior in the far wake of the wind turbine, the mean wake velocity profile scaled with centerline wake velocity deficit $\frac{\bar{u}-U_\infty}{\overline{U_s}}$ is plotted in self similarity coordinates $\eta = r/\delta$, for the case of 0.1% ambient turbulence level and $U_\infty = 10\ m/s$, in Figure 9.

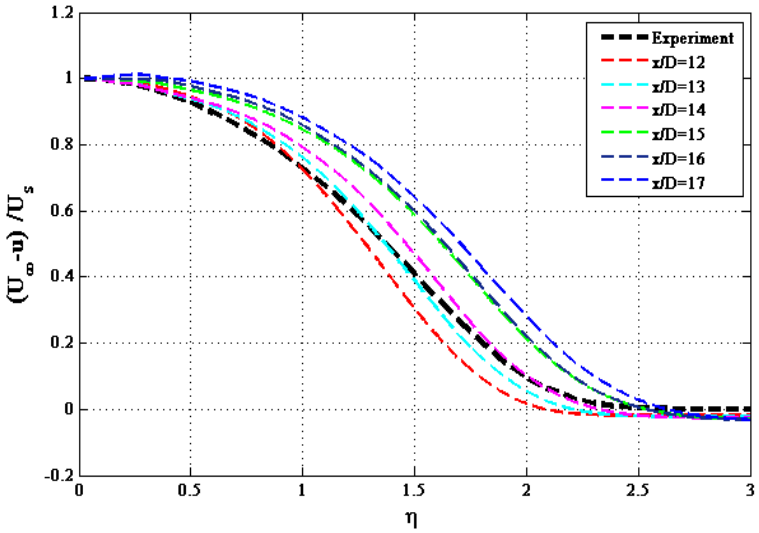

Figure 10: Mean wake velocity profile, scaled with centerline wake velocity deficit in self-preservation coordinate, (compared with the result shown in [2]).

In Figure 10, the numerical results are compared with a fitted curve to the experimental results which have been shown in [2] (black dashed line). However in the mentioned reference Johansson et al. argued that this trend is independent of the generator and should be similar for all cases. Figure 10 shows that the trends at different distances behind the wind turbine are in good agreement with the black dashed line. Therefore, it can be concluded that the mean velocity profile of the wake behind a wind turbine when scaled by centerline wake velocity deficit can reach the self-similarity state in the far wake region. However, the graphs do not collapse to a unique curve. This might be due to the presence of the pressure gradients even in the far wake which may lead to a small deviation of the above graphs, as the wake moves downstream.

4. Conclusion

The aim of this study was to improve the classical analytical model for estimating the rate of wake expansion and the decay of the wake velocity deficit in the far wake region behind a wind turbine. Therefore, in the theoretical approach, the flow parameters for a fully turbulent axisymmetric far wake were derived by applying the mass and momentum conservations, Reynolds shear stress, self- similarity assumption and utilizing the eddy viscosity closure. The theoretical approach was validated based on the results obtained from simulations that combine large eddy simulations with the actuator line technique for $0.1\%,\ 3\%, \text{and}\ 6\%$ ambient turbulence level and $U_\infty = 7 \text{ and } 10\ m/s$. The effect of ambient turbulence level and thrust coefficient on the wake recovery was investigated and the rate of wake expansion, and the decay of the wake velocity deficit was verified for 0.1%, 3% ambient turbulence level and $U_\infty = 10\ m/s$, and 0.1% ambient turbulence level and $U_\infty = 7\ m/s$. The results show that the time average of the wake velocity profile for a relatively long time domain will lead to axisymmetric and steady sate condition of the wake profile in a far wake region. The

nonlinear term of the velocity in the momentum equation in the far wake region cannot be neglected compared to the linear term, for low ambient turbulence level and high thrust coefficients. Therefore the theoretical determination of the powers for the wake expansion and the decay of the wake velocity deficit may not be valid in the case of the wake generated behind a wind turbine and low ambient turbulence level and high thrust coefficients. However, faster recovery of the wake by increasing the ambient turbulence level or decreasing the ambient wind velocity (higher thrust coefficients) will increase the differences between the linear and nonlinear terms of the momentum equations at certain distances behind the wind turbine, which will give closer powers for the decay of centerline wake velocity deficit and the expansion of half walk width, compared to the one predicted by the theoretical approach. In addition, the mean velocity profile of the wake behind a wind turbine, when scaled by the centerline wake velocity deficit, will reach the self-similarity state in a far wake region and low ambient turbulence level and high thrust coefficients.

Acknowledgement

This work was partly supported by the international project (DSF Sagsnr. 10-094544) under Danish Council for Strategic Research, Ministry of Science, Innovation and Higher Education, the Danish Council for Strategic Research for the project ' Center for Computational Wind Turbine Aerodynamics and Atmospheric Turbulence' (grant 2104-09-067216/DSF), (COMWIND) (http://www.comwind.mek.dtu.dk/Partners.aspx) , the Nordic Consortium on Optimization and Control of Wind Farms (http://picard.hgo.se/~nordwind/), which has provided access to the National Supercomputer Centre in Sweden (NSC), and Oticon Foundation.

References

[1] George, W.K., The self-preservation of turbulent flows and its relation to initial conditions and coherent structures. Advances in Turbulence, 1989: p. 39-73.

[2] Johansson, P.B.V., W.K. George, and M.J. Gourlay, Equilibrium similarity, effects of initial conditions and local Reynolds number on the axisymmetric wake. PHYSICS OF FLUIDS, 2003. 15(PART 3): p. 603-617.

[3] Johansson, P.B.V., The axisymmetric turbulent wake. 2002: Department of Thermo and Fluid Dynamics, Chalmers University of Technology.

[4] Johansson, P.B.V. and W.K. George, The far downstream evolution of the high-Reynolds-number axisymmetric wake behind a disk. Part 1. Single-point statistics. Journal of Fluid Mechanics, 2006. 555: p. 363-386.

[5] Cannon, S.C., Large-scale structures and the spatial evolution of wakes behind axisymmetric bluff bodies. 1991.

[6] Gourlay, M.J., et al., Numerical modeling of initially turbulent wakes with net momentum. PHYSICS OF FLUIDS, 2001. 13: p. 3783.

[7] Crespo, A., J. Hernandez, and S. Frandsen, Survey of modelling methods for wind turbine wakes and wind farms. Wind energy, 1999. 2(1): p. 1-24.

[8] Vermeer, L.J., J.N. Sørensen, and A. Crespo, Wind turbine wake aerodynamics. Progress in aerospace sciences, 2003. 39(6): p. 467-510.

[9] Lissaman PBS. Energy effectiveness of arbitrary arrays of wind turbine, in AIAA paper 79-0114, 1979. P.1-7

[10] Jensen, N.O., A note on wind generator interaction. 1983.

[11] Katic, I., et al., A Simple Model for Cluster Efficiency. EWEC'86. Proceedings. Vol. 1, 1987: p. 407-410.

[12] Larsen, G.C., A simple wake calculation procedure. 1988.

[13] Larsen, G.C., et al. Wind Fields in Wakes. in EWEC 1996 Proceedings. 1996. Goteborg (Sweden).

[14] Frandsen, S., et al., Analytical modelling of wind speed deficit in large offshore wind farms. Wind energy, 2006. 9: p. 39-53.

[15] Nasrin Arjomand Kermani, Analysis of turbulent wake behind a wind turbine, Master thesis, October 2012, Technical University of Denamk.

[16] Sørensen J. N., a.S.W.Z. Computation of wind tubine wakes using combined Novier Stokes/Actuator-Line Methodology. in the European Wind Energy Conferance EWEC 1999. Nice, Italy.

[17] Sørensen N.N, General Purpose Flow Solver Applied to flow over Hills in Risø, National labratory. 1995, Technical University of Denmark , Røskilde, Denmark.

[18] Michelsen, J.A., Basic 3D-A plat-Form for Development of multi block PDE solver. 1994, Department of luid mechanic, technical univerity of Denmark, DTU.

[19] Sørensen, N.N., General purpose flow solver applied to flow over hills. 1995: Risø¸ National Laboratory.

[20] Troldborg, N., J.N. Sørensen, and R. Mikkelsen. Actuator line simulation of wake of wind turbine operating in turbulent inflow. in Journal of Physics: Conference Series. 2007: IOP Publishing.

[21] Mann, J., Wind field simulation. Probabilistic engineering mechanics, 1998. 13(4): p. 269-282.

[22] MathWorks. [cited; Available , from: http://www.mathworks.se/help/optim/ug/lsqcurvefit.html.